Chinese Chemical Letters 36 (2025) 110256

Contents lists available at ScienceDirect

Chinese Chemical Letters

journal homepage: www.elsevier.com/locate/cclet

β-$Pb_3P_2S_8$: A new optical crystal with exceptional birefringence effect

Weiping Guo[a,b], Ying Zhu[a,b], Hong-Hua Cui[c,*], Lingyun Li[a,*], Yan Yu[a,*], Zhong-Zhen Luo[a,b,*], Zhigang Zou[a,b,d]

[a] Key Laboratory of Eco-materials Advanced Technology, Key Laboratory of Advanced Materials Technologies International (HongKong Macao and Taiwan) Joint Laboratory on Advanced Materials Technologies, College of Materials Science and Engineering, Fuzhou University, Fuzhou 350108, China
[b] Fujian Science & Technology Innovation Laboratory for Optoelectronic Information of China, Fuzhou 350108, China
[c] Mechanical and Electrical Engineering Practice Center, Fuzhou University, Fuzhou 350108, China
[d] Eco-materials and Renewable Energy Research Center, College of Engineering and Applied Sciences, Nanjing University, Nanjing 210093, China

ARTICLE INFO

Article history:
Received 30 May 2024
Revised 22 June 2024
Accepted 15 July 2024
Available online 15 July 2024

Keywords:
Birefringent crystals
Optical properties
Chalcogenides
β-$Pb_3P_2S_8$
Structural anisotropic

ABSTRACT

Birefringent crystals play an irreplaceable role in optical systems by adjusting the polarization state of light in optical devices. This work successfully synthesized a new thiophosphate phase of β-$Pb_3P_2S_8$ through the high-temperature solid-state spontaneous crystallization method. Different from the cubic α-$Pb_3P_2S_8$, the β-$Pb_3P_2S_8$ crystallizes in the orthorhombic *Pbcn* space group. Notably, β-$Pb_3P_2S_8$ shows a large band gap of 2.37 eV in lead-based chalcogenides, wide infrared transparent window (2.5−15 μm), and excellent thermal stability. Importantly, the experimental birefringence shows the largest value of 0.26@550 nm in chalcogenides, even larger than the commercialized oxide materials. The Barder charge analysis result indicates that the exceptional birefringence effect is mainly from the Pb^{2+} and S^{2-} in the [PbS_n] polyhedrons. Meanwhile, the parallelly arranged polyhedral layers could improve the structural anisotropic. Therefore, this work supports a new method for designing chalcogenides with exceptional birefringence effect in the infrared region.

Birefringent crystals are a critical type of optoelectronic materials that are used to regulate and detect the polarization state of light in optical devices. It is widely used in laser polarization technology, optical isolators, optical communications, phase compensators, *etc.* [1-6]. Over the past few years, several birefringent crystals have been commercially used, including YVO_4 (0.204@532 nm) [7], TiO_2 (0.256@546 nm) [8], $CaCO_3$ (0.172@532 nm) [9], $LiNbO_3$ (0.074@546 nm) [10], and α-BaB_2O_4 (0.122@546 nm) [11]. However, these crystals have significant disadvantages, such as the defects and impurities in $CaCO_3$ and TiO_2 crystals. The high production costs for YVO_4, $LiNbO_3$, and α-BaB_2O_4. Thus, new birefringent crystals with the advantages of high birefringence, large transmittance range, and good physical and chemical stability are urgently desired.

Chalcogenides are widely used as optical function materials since they have a wide infrared (IR) transmittance range covering the important atmospheric windows (3−5 and 8−12 μm) [12-17]. However, very few reports of chalcogenide birefringent crystals can be commercially applied. The main question is that the measured birefringence value difficultly reaches the level of oxide crystals. Meanwhile, the strong absorption in the IR waveband limited the application of oxide crystals. Therefore, looking for a new chalcogenide with large birefringence is a current research focus. It has widely been received that the birefringence value is related to the structural anisotropy of the crystal. Large structure anisotropy is the benefit of obtaining the large birefringence [18-20]. At present, the improvement of birefringence can be achieved by introducing highly anisotropic functional motifs, such as the planar triangle arrangement of [BS_3] and [B_3S_6] units in the thioborate system, the Pb^{2+}, Sn^{2+}, and Sb^{3+} with stereochemical active lone pair, the transition metal d^0 cations V^{5+}, Ti^{4+}, and Nb^{5+} with octahedron coordination [21-23]. These motifs could play a critical role in the birefringence. For example, the $NaBaBS_3$ with the π-conjugated [BS_3] planar unit features a birefringence of 0.177 at 550 nm [24]. The β-$BaGa_2Se_4$ with strong structure anisotropy of one dimensional (1D) $[GaSe_2]_\infty$ chain exhibits a large experimental birefringence of 0.18 at 550 nm [25]. The band gap (E_g) is also an important parameter for an optical material, which determines the transmittance cutoff edge in the application. Meanwhile, the thiophosphate with strong electronegativity in the P−S bond could benefit from obtaining the large E_g. In addition, designing compounds

* Corresponding authors.
E-mail addresses: hhcui@fzu.edu.cn (H.-H. Cui), lilingyun@fzu.edu.cn (L. Li), yuyan@fzu.edu.cn (Y. Yu), zzluo@fzu.edu.cn (Z.-Z. Luo).

https://doi.org/10.1016/j.cclet.2024.110256
1001-8417/

Table 1
Crystal information and structure refinement data for β-$Pb_3P_2S_8$.

Empirical formula	β-$Pb_3P_2S_8$
Formula weight	939.99
Crystal system	Orthorhombic
Space group	*Pbcn*
a/Å	12.8708(8)
b/Å	9.6073(6)
c/Å	10.2685(7)
Volume/Å^3	1269.74(14)
Z	4
ρ_{cal} (g/cm^3)	4.917
μ/mm^{-1}	41.198
F(000)	1316.0
Crystal size/mm^3	0.1 × 0.15 × 0.06
Radiation	Mo K$_\alpha$ (λ = 0.71073)
Goodness-of-fit on F^2	1.114
Completeness	100%
Largest diff. peak and hole	1.76/−3.24
R_1, wR_2 [$I > 2\sigma(I)$][a]	R_1 = 0.0349, wR_2 = 0.0683
R_1, wR_2 (all data)	R_1 = 0.0369, wR_2 = 0.0693

[a] $R_1 = \Sigma||F_o| - |F_c||/\Sigma|F_o|$, $wR_2 = \{\Sigma w[(F_o)^2 - (F_c)^2]^2/\Sigma w[(F_o)^2]^2\}^{1/2}$.

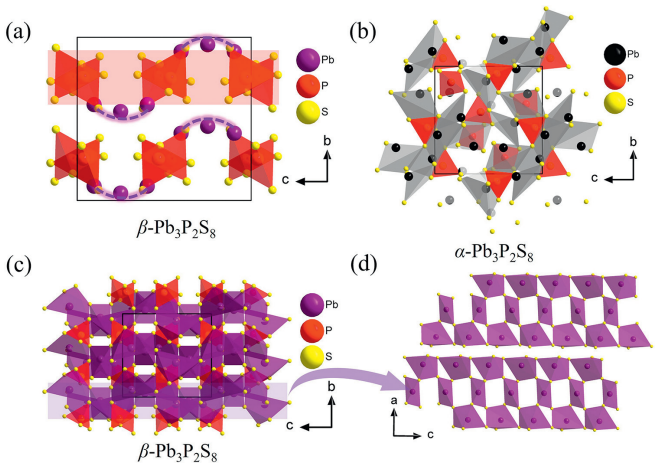

Fig. 1. Crystal structures of β-$Pb_3P_2S_8$ and α-$Pb_3P_2S_8$: (a) The arrangement of [PS_4] tetrahedra and Pb atoms in β-$Pb_3P_2S_8$ along the *a*-axis. (b) The whole structure framework diagram of α-$Pb_3P_2S_8$ along the *a*-axis. (c) The whole structure framework diagram of β-$Pb_3P_2S_8$ along the *a*-axis. (d) The $[Pb_3S_4]_\infty$ polyhedral layer in β-$Pb_3P_2S_8$.

with few components is beneficial to the growth of single crystals. Therefore, based on the thiophosphate system, introducing the anisotropic structure units is a feasible way to obtain optical material with large birefringence.

This work introduced the highly electronegativity P^{5+} and $6s^2$ lone-pair electrons of Pb^{2+} into the Pb−P−S system [26-28]. A new lead-based thiophosphate phase of β-$Pb_3P_2S_8$, was obtained by the high-temperature solid-state spontaneous crystallization method. The β-$Pb_3P_2S_8$ crystallizes in the orthorhombic space group, while the other phase of known α-$Pb_3P_2S_8$ belongs to the cubic crystal system [29]. As we know, the cubic system is optically isotropic. Therefore, the birefringence of α-$Pb_3P_2S_8$ is zero. Meanwhile, the consistent arranged [PbS_n] polyhedral layers in β-$Pb_3P_2S_8$ could effectively increase the structural anisotropy, while the arrangement mode in α-$Pb_3P_2S_8$ is irregular. The orthorhombic phase of β-$Pb_3P_2S_8$ realizes the decrease of symmetry, which can be a candidate as the birefringence crystal. Due to the introduction of high electronegativity P^{5+}, the β-$Pb_3P_2S_8$ possesses a moderate E_g (2.37 eV) in the thiophosphate-based compounds optical crystal system. The IR spectrum and thermogravimetric analysis measurements indicate that β-$Pb_3P_2S_8$ has a wide transmittance range and excellent thermal stability. In addition, the birefringence measurement was performed by a polarizing microscope. This crystal has an exceptional birefringence effect of 0.26@550 nm, which is the largest value for experiment-reported chalcogenides and larger than that of commercialized birefringent crystals. Furthermore, the theoretical calculation of birefringence (0.23@550 nm) is close to the experimental value, demonstrating the accuracy of the test. The exceptional birefringence effect can be attributed to the collaborative contribution between lone-pair electrons of Pb^{2+} and parallelly arranged polyhedral layers in β-$Pb_3P_2S_8$.

The β-$Pb_3P_2S_8$ crystallizes in the orthorhombic centrosymmetry *Pbcn* space group with unit cell parameters of a = 12.8708(8) Å, b = 9.6073(6) Å, c = 10.2685(7) Å, V = 1269.74(14) Å^3, and Z = 4. There are two crystallography unique Pb atoms (Wyckoff sites: 8d and 4c), one P atom (Wyckoff site: 8d), and four S atoms (Wyckoff site: 8d) in an asymmetric unit. The detailed crystal refinement data for β-$Pb_3P_2S_8$ is shown in Table 1. The bond valance calculations (Pb: 1.760−1.797; P: 5.301; S: 1.524−2.053) indicate that Pb, P, and S atoms are in valence states of +2, +5, and −2 (Table S1 in Supporting information), which confirms that the reasonable structure solution. The bond lengths of Pb−S range from 2.846(3) Å to 3.231(3) Å (Table S3 in Supporting information), which is consistent with some known Pb-based sulfides, such as $PbGa_4S_7$ (Pb−S: 2.742(3)−3.533(3) Å) [30], $Pb_4Ga_4GeS_{12}$ (Pb−S: 2.827(5)−3.375(4) Å) [31] and PbU_2S_5 (Pb−S: 2.786(16)−3.103(16) Å) [32]. The bond lengths of P−S are range from 2.014(5) Å to 2.068(4) Å (Table S3), which is consistent with the $CuHgPS_4$ (P−S: 2.056(3)−2.061(3) Å) [33], $Eu_2P_2S_6$ (P−S: 1.979(6)−2.061(6) Å) [26], and $Hg_3P_2S_8$ (P−S: 2.036(5)−2.080(5) Å) [34]. In order to better describe the structural characteristics, we only considered Pb−S bonds with lengths less than 3.11 Å as [PbS_n] polyhedrons. As shown in Fig. 1a and Fig. S1 (Supporting information), the crystal structure of β-$Pb_3P_2S_8$ is composed of [Pb(1)S_5] tetragonal pyramid, [Pb(2)S_4] distorted tetrahedron, and [PS_4] tetrahedron. The [PS_4] tetrahedra are arranged in reverse parallel pairs in the *ac* plane while not connected with each other (red-shaded area). The [PS_4] tetrahedra are edge-shared and vertex-shared with [Pb(1)S_5] tetragonal pyramids and [Pb(2)S_4] tetrahedra (Fig. S12a in Supporting information), forming the 3D structure (Fig. 1c), eventually.

As displayed in Fig. 1b and Fig. S1, the α-$Pb_3P_2S_8$ is composed of [PS_4] and [Pb(1)S_4] tetrahedra. The [PS_4] tetrahedra are edge-shared with [Pb(1)S_4] tetrahedra forming the 3D structure (Fig. S12b in Supporting information). At the same time, the inconsistent arrangement of basic build units (BBUs) is not conducive to improving the structural anisotropy. And α-$Pb_3P_2S_8$ belongs to the cubic system, which has no optical anisotropy. However, in the structure of β-$Pb_3P_2S_8$, the BBUs rank more regularly along the *b*-axis direction. As shown in Fig. 1d, the [Pb(1)S_5] tetragonal pyramids are vertex-shared with [Pb(2)S_4] tetrahedra forming the $[Pb_3S_4]_\infty$ polyhedral layer in *ac* plane. Eventually, the alternately arranged $[Pb_3S_4]_\infty$ polyhedral layers and [PS_4] tetrahedra improve the optical anisotropy in β-$Pb_3P_2S_8$ (Fig. 1c).

The polycrystalline of β-$Pb_3P_2S_8$ was synthesized through the high-temperature solid-state spontaneous crystallization method with additional Cu. However, Cu does not participate in the synthesis of the Pb−P−S system and produces the by-product of Cu_3PS_4. The Cu may act as a cocatalyst in the synthesis process. A similar situation was also reported in $Cs_5Ga_9S_{16}$, $RbGa_5S_8$, $CsGa_5S_8$, and $CsLiGa_6S_{10}$ with the additional elements added before the synthesis [35-37]. In addition, the synthesis process of known α-$Pb_3P_2S_8$ was grown by the two-step vapor transport reaction in a gradient furnace with I_2 transport agent [29]. The synthesis method is completely different for them. The β-$Pb_3P_2S_8$ phase was tested by powder X-ray diffraction (XRD) measurement (Fig. S2 in Supporting information), in which the experimental XRD curve matched

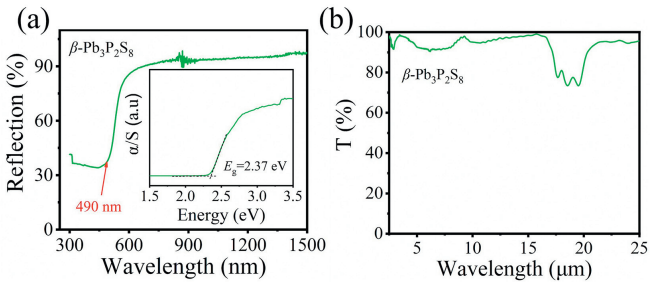

Fig. 2. (a) The experimental E_g from UV–vis-near infrared diffuse reflection spectrum of β-$Pb_3P_2S_8$ and (b) IR spectrum measurement of β-$Pb_3P_2S_8$.

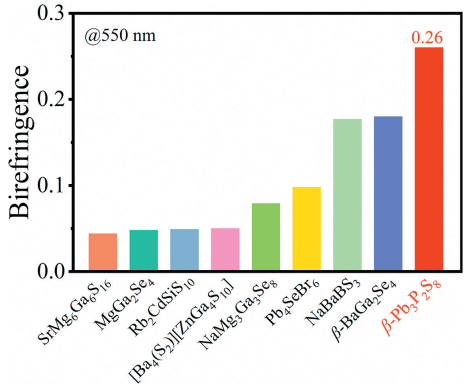

Fig. 3. Compared with the reported experimental birefringence values in the chalcogenides at 550 nm.

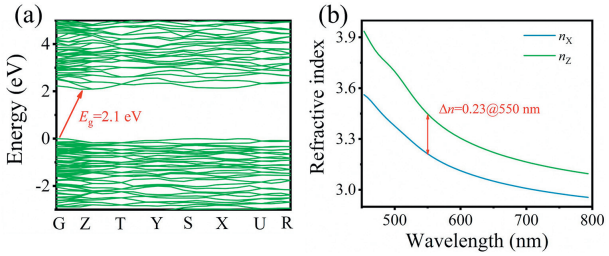

Fig. 4. (a) Calculated electronic band structure of β-$Pb_3P_2S_8$ and (b) the calculated refractive index curves of β-$Pb_3P_2S_8$.

well with the simulated XRD curve of β-$Pb_3P_2S_8$ phase calculated from the Crystallographic Information File (CIF). The diffraction peaks do not match the simulated α-$Pb_3P_2S_8$ phase, indicating the successfully synthesized new β-$Pb_3P_2S_8$ phase. In addition, the phase purity was measured by the refined powder XRD for β-$Pb_3P_2S_8$ (Fig. S3 in Supporting information). The energy-dispersive spectrum (EDS) result is shown in Fig. S4 (Supporting information). The Pb, P, and S elements were detected and distributed uniformly on a single crystal surface. The ratio of elements is 2.95:2:7.85, close to the chemical formula of β-$Pb_3P_2S_8$. In addition, the Raman spectrum of β-$Pb_3P_2S_8$ is presented in Fig. S5 (Supporting information), in which the peaks at 379 cm^{-1} and 561 cm^{-1} belong to the vibration modes of the P–S bond, the absorption peaks at 195 cm^{-1} and 248 cm^{-1} could be assigned to the Pb–S bond vibration.

The thermogravimetric (TG) analysis of β-$Pb_3P_2S_8$ was measured from 300 K to 1273 K under the N_2 atmosphere. As shown in Fig. S6 (Supporting information), the β-$Pb_3P_2S_8$ is stabilized to 990 K and has begun to decompose. The differential thermal analysis (DTA) curve shows an endothermic peak at 1099 K, indicating the phase decomposition behavior of β-$Pb_3P_2S_8$. In order to measure the phase stability of β-$Pb_3P_2S_8$ with temperature change, the differential scanning calorimetry (DSC) and temperature-dependent XRD measurements were executed. As shown in Fig. S7 (Supporting information), the heating and cooling DSC curves show no endothermic or exothermic peak from 300 K to 773 K, indicating the non-phase transition behavior for β-$Pb_3P_2S_8$. Meanwhile, the temperature-dependent XRD measurement in Fig. S8 (Supporting information) shows that the β-$Pb_3P_2S_8$ has the same diffraction peaks from 300 K to 723 K, also indicating the irreversible phase transition between the α- and β-$Pb_3P_2S_8$. The UV–vis-NIR diffuse reflection spectrum for β-$Pb_3P_2S_8$ was collected by the polycrystalline powder displayed in Fig. 2a. The reflection spectrum indicates that β-$Pb_3P_2S_8$ has moderate visible light transmittance (including 550 nm). The experimental E_g result is approximately 2.37 eV in accordance with the orange color of the crystal, converted by the Kubelka-Munk function. Compared with the E_g in the lead-based chalcogenides optical crystal system (Table S5 in Supporting information), the β-$Pb_3P_2S_8$ has a large E_g and attains the requirement for optical material. The IR spectrum is shown in Fig. 2b with no obvious absorption peak between 2.5–15 μm, which indicates that β-$Pb_3P_2S_8$ has high IR transmittance and covers the two critical atmospheric windows of 3–5 and 8–12 μm. However, the IR transmittance spectra for the pressed pellet of "KBr + powder" samples are always wider than the single crystals [38]. The larger and higher quality of β-$Pb_3P_2S_8$ single crystals need to be synthesized to obtain the accurate transmittance spectrum.

The birefringence of β-$Pb_3P_2S_8$ was measured by the polarizing microscope. One smooth plate single crystal was selected for testing. As shown in Fig. S10 (Supporting information), the β-$Pb_3P_2S_8$ achieves complete extinction under the orthogonal polarized light. The optical path difference (R) was tested to be 2.471 μm with a thickness (T) of 9.33 μm. The measured crystal face is (001), which was determined by the single crystal diffractometer (Fig. S9 in Supporting information). According to the birefringence calculated formula of $R = |N_e - N_o| \times T = \Delta n \times T$ [39], the experimental birefringence value of β-$Pb_3P_2S_8$ is calculated to be 0.26. Because the measured crystal face may not be the most anisotropic in the structure, the actual birefringence of β-$Pb_3P_2S_8$ is larger than or equal to 0.26@550 nm. Interestingly, it surpasses the commercialized birefringence materials at present, such as $CaCO_3$ (0.172@532 nm) [9], YVO_4 (0.204@532 nm) [7], α-BaB_2O_4 (0.122@532 nm) [11], and TiO_2 (0.256@546 nm) [8]. Meanwhile, compared with the reported experimental birefringence of the chalcogenides system (Fig. 3) [24,25,40-45], the β-$Pb_3P_2S_8$ possesses the highest birefringence in the chalcogenides under 550 nm. It demonstrates the huge potential for application as a newly birefringence crystal.

In order to further comprehend the origin of the optical properties in the structure, the first-principles calculations based on the density function theory (DFT) method were performed in the Cambridge Sequential Total Energy Package (CASTEP). As shown in Fig. 4a, the electronic band structural calculation result indicates that β-$Pb_3P_2S_8$ is an indirect band gap compound of 2.1 eV with valence band maximum (VBM) and conduction band minimum (CBM) situated at G and Z points, respectively. The calculated result shows the difference from the experimental value of 2.37 eV, caused by the discontinuity of exchange-correlation energy [46]. In addition, the calculated birefringence in Fig. 4b shows that β-$Pb_3P_2S_8$ has a large value of 0.23@550 nm, consistent with the experimental result. The calculated total density of states (DOS) and partial density of states (PDOS) are shown in Fig. S14 (Supporting information). The VBM is mainly dominated by S-3p orbital, Pb-6s orbital, and Pb-6p orbital. In comparison, the major contribution of the CBM is from the S-3p orbital and the Pb-6p orbital, with

little from the P-3p orbital. Therefore, the Pb-6p orbital and S-3p orbital concentrated on the VBM and CBM stands for the strong hybridization between [PbS_n] polyhedrons, indicating that the optical properties of β-$Pb_3P_2S_8$ are mainly determined by Pb−S bond. In addition, a method of Barder charge analysis was used to evaluate the concrete birefringence contributions of ions for β-$Pb_3P_2S_8$ [47]. As a result, the Pb^{2+} contributes 28.56% to birefringence, S^{2-} contributes 71.68% to birefringence, but P^{5+} produces the opposite contribution of −0.24% to birefringence. Thus, it shows that [PbS_n] polyhedron plays a vital role in the birefringence of β-$Pb_3P_2S_8$.

In summary, a new thiophosphate phase of β-$Pb_3P_2S_8$ was synthesized by the high-temperature solid-state method to meet the requirement of birefringent crystals in the infrared band. The β-$Pb_3P_2S_8$ exhibits a large E_g ~2.37 eV in the lead-based chalcogenides system, a wide infrared transparent window (2.5−15 μm), and excellent thermal stability. In comparison, the arrangement of structural units in α-$Pb_3P_2S_8$ is irregular, deteriorating the structural anisotropy. On the contrary, the parallelly arranged $[Pb_3S_4]_\infty$ polyhedral layers in β-$Pb_3P_2S_8$ improve structural anisotropy. The exceptional birefringence effect of β-$Pb_3P_2S_8$ is 0.26@550 nm, which is the highest value in reported chalcogenides. The result of the theoretical calculation is consistent with the experimental birefringence. The Barder charge analysis shows that Pb^{2+} and S^{2-} contribute mainly to birefringence, indicating the strong hybridization of [PbS_n] polyhedrons. More importantly, the strong anisotropy of polyhedron layered stack structure offers a new viewpoint to the design and synthesis of chalcogenides with exceptional birefringence effect.

Declaration of competing interest

The authors declare no competing financial interest.

CRediT authorship contribution statement

Weiping Guo: Writing – original draft, Methodology, Investigation, Data curation. **Ying Zhu:** Methodology, Investigation. **Hong-Hua Cui:** Investigation, Formal analysis, Conceptualization. **Lingyun Li:** Writing – review & editing, Supervision, Methodology, Investigation, Conceptualization. **Yan Yu:** Writing – review & editing, Resources, Funding acquisition, Conceptualization. **Zhong-Zhen Luo:** Writing – review & editing, Supervision, Resources, Methodology, Funding acquisition, Data curation, Conceptualization. **Zhigang Zou:** Resources, Project administration, Funding acquisition, Conceptualization.

Acknowledgments

This study was supported in part by the National Natural Science Foundation of China (No. 52102218), the National Key Research and Development Program of China (No. 2020YFA0710303), and the Fujian Science & Technology Innovation Laboratory for Optoelectronic Information of China (No. 2021ZZ127). The authors acknowledge the Minjiang Scholar Professorship (No. GXRC-21004) and the Natural Science Foundation of Fujian Province of China (No. 2021J01594). The authors thank Prof. Sangen Zhao at Fujian Institute of Research on the Structure of Matter for helping with the birefringence measurement.

Supplementary materials

Supplementary material associated with this article can be found, in the online version, at doi:10.1016/j.cclet.2024.110256.

References

[1] S. Niu, G. Joe, H. Zhao, et al., Nat. Photonics 12 (2018) 392–396.
[2] X. Chen, W.G. Lu, J. Tang, et al., Nat. Photonics 15 (2021) 813–816.
[3] S. Han, A. Tudi, W. Zhang, et al., Angew. Chem. Int. Ed. 62 (2023) e202302025.
[4] Z.Y. Xie, L.G. Sun, G.Z. Han, et al., Adv. Mater. 20 (2008) 3601–3604.
[5] Y. Feng, R. Chen, J. He, et al., Nat. Commun. 14 (2023) 6739.
[6] S.A. Dereshgi, T.G. Folland, A.A. Murthy, et al., Nat. Commun. 11 (2020) 5771.
[7] H.T. Luo, T. Tkaczyk, E.L. Dereniak, et al., Opt. Lett. 31 (2006) 616–618.
[8] J.R. DeVore, J. Opt. Soc. Am. 41 (1951) 416–419.
[9] G. Ghosh, Opt. Commun. 163 (1999) 95–102.
[10] D.E. Zelmon, D.L. Small, D. Jundt, J. Opt. Soc. Am. B 14 (1997) 3319–3322.
[11] Z. Guoqing, X. Jun, C. Xingda, et al., J. Cryst. Growth 191 (1998) 517–519.
[12] Y. Chu, H. Wang, T. Abutukadi, et al., Small 19 (2023) e2305074.
[13] Z.Z. Luo, C.S. Lin, H.H. Cui, et al., Chem. Mater. 26 (2014) 2743–2749.
[14] M.M. Chen, S.H. Zhou, W. Wei, et al., ACS Mater. Lett. 4 (2022) 1264–1269.
[15] W. Wang, D. Mei, F. Liang, et al., Coord. Chem. Rev. 421 (2020) 213444.
[16] W.F. Chen, B.W. Liu, S.M. Pei, et al., Adv. Sci. 10 (2023) 2207630.
[17] J.J. Xu, K. Wu, Coord. Chem. Rev. 486 (2023) 215139.
[18] J.H. Wu, C.L. Hu, T.K. Jiang, et al., J. Am. Chem. Soc. 145 (2023) 24416–24424.
[19] Z. Wang, X. Chen, Y. Song, et al., Angew. Chem. Int. Ed. 62 (2023) e202311086.
[20] Y. Li, X. Zhang, J. Zheng, et al., Angew. Chem. Int. Ed. 62 (2023) e202304498.
[21] T. Fu, K. Bu, X. Sun, et al., J. Am. Chem. Soc. 145 (2023) 16828–16834.
[22] J. Guo, A. Tudi, S. Han, et al., Angew. Chem. Int. Ed. 60 (2021) 24901–24904.
[23] H. Yu, M.L. Nisbet, K.R. Poeppelmeier, J. Am. Chem. Soc. 140 (2018) 8868–8876.
[24] Y. Yun, W. Xie, Y. Huang, et al., Chem. Mater. 34 (2022) 5215–5223.
[25] Y. Zhang, Q. Bian, H. Wu, et al., Angew. Chem. Int. Ed. 61 (2022) e202115374.
[26] X. Huang, S.H. Yang, X.H. Li, et al., Angew. Chem. Int. Ed. 61 (2022) e202206791.
[27] Z.Z. Luo, C.S. Lin, H.H. Cui, et al., Chem. Mater. 27 (2015) 914–922.
[28] Z. Li, J. Yao, Y. Wu, Cryst. Growth Des. 20 (2020) 7550–7564.
[29] B. Ji, E. Guderjahn, K. Wu, et al., PCCP 23 (2021) 23696–23702.
[30] X. Li, L. Kang, C. Li, et al., J. Mater. Chem. C 3 (2015) 3060–3067.
[31] W. Yin, A.K. Iyer, C. Li, et al., J. Solid State Chem. 241 (2016) 131–136.
[32] J. Prakash, M.S. Tarasenko, A. Mesbah, et al., Inorg. Chem. 53 (2014) 11626–11632.
[33] M.Y. Li, Z. Ma, B. Li, et al., Chem. Mater. 32 (2020) 4331–4339.
[34] Y. Chu, P. Wang, H. Zeng, et al., Chem. Mater. 33 (2021) 6514–6521.
[35] J.X. Zhao, X.M. Jiang, W.F. Chen, et al., Inorg. Chem. Front. 9 (2022) 4624–4631.
[36] W.F. Chen, X.M. Jiang, S.M. Pei, et al., Sci. China Mater. 66 (2023) 740–747.
[37] Z. Wang, B.W. Liu, G.-C. Guo, Inorg. Chem. Front. 9 (2022) 6554–6560.
[38] X. Luo, Z. Li, Y. Guo, et al., J. Solid State Chem. 270 (2019) 674–687.
[39] W. Huang, X. Zhang, Y. Li, et al., Angew. Chem. Int. Ed. 61 (2022) e202202746.
[40] J. Chen, Y. Zhang, H. Wu, et al., Adv. Opt. Mater. 11 (2023) 2202147.
[41] P. Wang, Y. Chu, A. Tudi, et al., Adv. Sci. 9 (2022) 2106120.
[42] J. Zhou, Z. Fan, K. Zhang, et al., Mater. Horiz. 10 (2023) 619–624.
[43] K. Ding, H. Wu, Z. Hu, et al., Small 19 (2023) 2302819.
[44] L. Luo, L. Wang, J. Chen, et al., J. Am. Chem. Soc. 144 (2022) 21916–21925.
[45] J. Wang, H. Wu, H. Yu, et al., Adv. Opt. Mater. 10 (2022) 2102673.
[46] R.W. Godby, M. Schlüter, L.J. Sham, Phys. Rev. B 36 (1987) 6497–6500.
[47] C.S. Lin, A.Y. Zhou, W.D. Cheng, et al., J. Phys. Chem. C 123 (2019) 31183–31189.